



# Chlorophyll-*a* estimations in complex coastal waters from space — A new optimization method by spatially resolved scaling factors

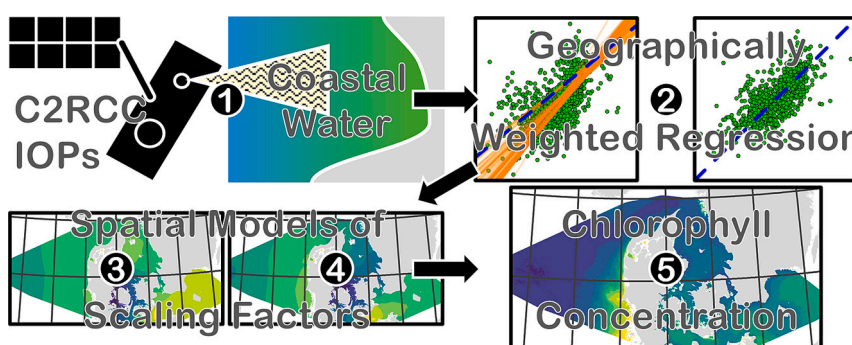
Andreas Holbach<sup>a,\*</sup>, Sanjina Upadhyay Stæhr<sup>a</sup>, Peter Anton Upadhyay Stæhr<sup>a</sup>, Stiig Markager<sup>a</sup>

<sup>a</sup> Aarhus University, Department of Ecoscience, Frederiksborgvej 399, 4000, Roskilde, Denmark

## HIGHLIGHTS

- Spatial optimization improves chlorophyll-*a* from Sentinel-3 OLCI C2RCC in coasts.
- GWR with cost-distance enables spatial scaling of phytoplankton absorption.
- Validation shows improved accuracy over default C2RCC chlorophyll estimates.
- Enables regionally tuned chlorophyll-*a* maps e.g. for Danish marine waters.
- Supports EU monitoring with regionally calibrated satellite chlorophyll data.

## GRAPHICAL ABSTRACT



## ARTICLE INFO

### Keywords:

Sentinel-3  
OLCI  
Geographically weighted regression (GWR)  
Inherent optical properties (IOPs)  
Eutrophication  
Remote sensing

## ABSTRACT

Accurate satellite-based monitoring of chlorophyll-*a* (*Chla*) in optically complex coastal waters remains a key challenge for ocean color remote sensing. This study presents a novel spatial optimization framework to improve *Chla* retrievals from Sentinel-3 OLCI level 2 products processed with the Case 2 Regional CoastColour (C2RCC) algorithm. This widely used operational satellite product targets complex coastal waters and is readily available for marine monitoring and management purposes, but for *Chla* showed rather poor performance, so far. Focusing on Danish marine waters in the North and Baltic Seas, we developed an innovative geographically weighted regression (GWR) approach accounting for hydrologically complex coastlines by using cost-distance metrics. Spatially resolved scaling factors linking satellite-derived phytoplankton absorption to *in situ* *Chla* concentrations from Denmark's national monitoring program (NOVANA) for the years 2018–2023 were derived. Validation using temporally independent subsets demonstrated that the GWR-derived scaling factors significantly improved agreement with *in situ* *Chla* data (*R* from 0.59 to 0.65), reducing root mean square error (RMSE from 0.29 to 0.27) relative to globally calibrated C2RCC products. The method is transparent, reproducible, operationally feasible, and outperforms the default C2RCC and OC4ME algorithms in both day-precise matchups and long-term averages. The resulting spatially continuous, regionally tuned *Chla* maps, support enhanced assessments of eutrophication and phytoplankton dynamics. This transferable framework contributes to advancing quantitative remote sensing in coastal environments and supports operational marine monitoring e.g. under EU directives.

\* Corresponding author.

E-mail address: [anho@ecos.au.dk](mailto:anho@ecos.au.dk) (A. Holbach).

<https://doi.org/10.1016/j.scitotenv.2025.180868>

Received 13 June 2025; Received in revised form 31 October 2025; Accepted 31 October 2025

Available online 12 November 2025

0048-9697/© 2025 The Authors. Published by Elsevier B.V. This is an open access article under the CC BY license (<http://creativecommons.org/licenses/by/4.0/>).

## 1. Introduction

Remote sensing of ocean color, particularly chlorophyll-*a* (*Chla*) concentrations, has emerged as a pivotal tool for advancing cost-effective and scalable marine monitoring strategies (Brockmann et al., 2016; Brockmann et al., 2004; Harvey et al., 2015). Remote sensing data can provide unparalleled insights into marine ecosystem dynamics across spatial and temporal scales that are unattainable through traditional *in situ* monitoring methods (Strong and Elliott, 2017; Toming et al., 2017).

A focus of marine *Chla* monitoring is eutrophication and (potentially harmful) algal blooms, both posing significant environmental challenges for coastal waters globally (Smith, 2003). Timescales of these phenomena range from short- (daily) to long-term (multi-year) events and trends. In the North and Baltic Seas, for example, assessments of eutrophication status (including *Chla* as eutrophication indicator) must be reported every 6th year according to EU directives (EU, 2000; EU, 2008; Staehr et al., 2023).

Complex coastal waters, such as the shallow near-coastal water bodies of the North and Baltic Seas, remain challenging for state-of-the-art spectral ocean color algorithms in remote sensing (Harvey et al., 2015; Pitarch et al., 2016; Staehr et al., 2023; Staehr et al., 2022; Toming et al., 2017). The European Space Agency (ESA) launched since 2016 two Sentinel-3 (S3) A&B satellites, equipped with the Ocean and Land Cover Instrument (OLCI). This spectral sensor records 21 channels between 400 and 1020 nm at a spatial resolution of ~300 m and revisiting time < 2 days in Danish latitudes (Cazzaniga et al., 2019). ESA operationally processes spectral images from OLCI with the Case 2 Regional CoastColour (C2RCC) processor, inverting reflectance spectra into inherent optical properties (IOPs) of phytoplankton pigments, colored organic matter, and suspended particles (Brockmann et al., 2016; Doerffer, 2010). C2RCC's neural network (NN) attributes absorption coefficients to phytoplankton pigments ( $a_{pig}^{443}$ ), as well as detritus and gelbstoff ( $a_{dg}^{443}$ ), and a scattering coefficient to total suspended matter (TSM,  $b_{tot}^{443}$ ), each at 443 nm (Brockmann et al., 2016). For pigments, the IOP is converted into *Chla* concentration in the level 2 product based upon empirical scaling factors (Doerffer, 2010; Doerffer and Embacher, 2016; ESA, 2020):

$$Chla = a_{pig}^{443} Chl_{exp} \times Chl_{fact} \quad (1)$$

where  $Chl_{exp} = 1.04$  and  $Chl_{fact} = 21.0$  are default settings to convert  $a_{pig}^{443}$  ( $m^{-1}$ ) into *Chla* ( $mg \cdot m^{-3}$ ) concentration. However, these scaling factors can be regionally variable (Brockmann et al., 2016).

This operational and widely used satellite product targets complex coastal waters and is readily available for marine monitoring and management purposes. Recent studies, however, have highlighted the limitations of using S3 OLCI level 2 (S3OL2) products, particularly from C2RCC, for *Chla* monitoring in optically complex Case 2 waters such as those found in the North and Baltic Seas. While several studies report overestimation of *Chla* in turbid or CDOM-rich waters — especially near river plumes (Tran et al., 2023) — others documented systematic underestimation in clearer waters or during low-biomass periods in the Baltic Sea, particularly when using default C2RCC settings (Hammond et al., 2020). For example, Kratzer and Plowey (2021) and Toming et al. (2017) found C2RCC underestimating *Chla* concentrations in the central Baltic Sea, likely due to insufficient representation of local optical conditions (Hammond et al., 2020). This is especially pronounced in shallow nearshore waters (Liu et al., 2021; Staehr et al., 2022, 2023). Similarly, Kutser et al. (2018) and Ligi et al. (2017) emphasized the need for regionally adapted algorithms to improve retrieval accuracy. A recent validation by O'Kane et al. (2024) further confirmed that applying global calibration schemes can degrade *Chla* accuracy in the Baltic. However, data-driven means for spatially continuous tuning of *Chla* products from C2RCC outputs are lacking.

For *Chla*, scaling factors in C2RCC relate  $a_{pig}^{443}$  to *Chla* concentration, based on the *Chla*-specific absorption coefficient of phytoplankton pigments. It is known that the *Chla*-specific absorption properties of phytoplankton pigments are widely variable, influenced by e.g. total *Chla* concentration, species composition, pigment packaging, accessory pigments, and size distribution of phytoplankton cells (Ciotti et al., 2002; Martin, 2014; Staehr and Markager, 2004; Staehr et al., 2004). Consequently, the applied scaling factors for the conversion of phytoplankton pigment absorption into *Chla* concentration likely require local adaptation to derive adequate and reliable estimates of *Chla* from S3OL2 products. Within the Sentinel Application Platform (SNAP) (Doerffer and Embacher, 2016; ESA, 2020), users can adjust these scaling factors for *Chla* retrieval for the entire area of interest (Kyryliuk and Kratzer, 2019). Thus, uncertainties and deviations in the S3OL2 *Chla* product will reflect inherent variability in *Chla*-specific absorption properties. A single set of scaling factors can hardly represent highly dynamic marine environments to derive *Chla* from  $a_{pig}^{443}$ .

In this study, we develop, validate, and apply an innovative purely spatial modelling approach, to optimize local scaling factors by aligning operational S3OL2 products with *in situ* *Chla* data from the operational national environmental monitoring program of Denmark (NOVANA) for the years 2018–2023. The approach is based on several key assumptions: (1) C2RCC reliably derives  $a_{pig}^{443}$ , (2) the scaling factors  $Chl_{exp}$  and  $Chl_{fact}$  are spatial variables, and (3) each point in space has a valid set of  $Chl_{exp}$  and  $Chl_{fact}$  relating  $a_{pig}^{443}$  with *Chla* concentration. Based on these assumptions, we hypothesize that geographically weighted regression (GWR) modelling (Charlton and Fotheringham, 2009) can approximate local scaling factors by analyzing matchups between S3OL2 data and *in situ* *Chla* samples. If successful, the methodological framework can be transferred and applied to other regions, satellite sensors, and parameters and support research and modern marine monitoring and management worldwide. We expect the spatial approach to significantly improve the agreement between satellite-based estimates of *Chla* and *in situ* measurements.

## 2. Materials and methods

This study builds upon a previous paper, where S3OL2 products were used to estimate light attenuation at the example of Danish marine waters (Holbach et al., 2025). Hence, the study area, spatial background data, set of S3OL2 images, and first steps of satellite data handling are exactly the same, but deviate after having retrieved the IOP  $a_{pig}^{443}$ .

### 2.1. Study area, spatial working grid and geographic data

The study area (Fig. 1) covers the transition from the open North Sea (a) through Skagerrak (b), Kattegat (b), the Belt Sea (e-g), and into the Baltic Sea (i). This area is an optically complex region with strong environmental gradients, such as salinity, colored dissolved organic matter (CDOM), nutrients, tidal dynamics, bathymetry, and hydrodynamics (Kowalczyk et al., 2006; Mélin and Vantrepotte, 2015; Pitarch et al., 2016; Riemann et al., 2015; Staehr et al., 2023). Numerous estuaries (fjords), bays, and straits further characterize the Danish coastline, with very specific ecological settings and phytoplankton communities (Hansen and Høgsund, 2021; Henriksen, 2009; Maar et al., 2016; Olli et al., 2011). Details on the spatial working grid, as well as spatial background data (Danish Agency for Climate Data, 2025; Danish Geodata Agency, 2024; EMOdnet Bathymetry Consortium, 2022) can be found in suppl. Information.

### 2.2. In situ *Chla* monitoring data

As part of the NOVANA monitoring program, *Chla* ( $\mu g \times L^{-1}$ ) is determined photometrically from filtered water samples (Markager and

Fossing, 2013). Data are stored in the Danish surface water database (ODA), which is publicly available (<https://odaforalle.au.dk/>). From ODA, we acquired all *Chla* values from an average depth of  $\leq 1$  m for the years 2018–2023. In total, 11,056 *Chla* values from 173 monitoring stations were received. *Chla* values were aggregated as daily averages per station, and we only kept values coinciding with valid bathymetry for the corresponding pixel of the working grid. This left 10,320 daily *Chla* values from 163 monitoring stations (Fig. 1).

In addition, we accessed a recently published global collection of phytoplankton spectral absorption coefficients, comprising 554 *in situ* datasets specifically generated for matchup analyses with S3OL2 data (Bracher et al., 2025a; Bracher et al., 2025b). From these data, we used absorption coefficients of phytoplankton at 442.5 nm.

### 2.3. Sentinel-3 OLCI level 2 water full-resolution products

Similar to Holbach et al. (2025), this study used S3OL2 data processed by EUMETSAT, including products from both the baseline atmospheric correction (BAC) and the alternative atmospheric correction (AAC) using the C2RCC algorithm. BAC products were designed for 'Open Waters, with a spectral signature dominated by phytoplankton pigments' (EUMETSAT, 2024). A relevant variable from the S3OL2-BAC products for this study is *Chla*<sup>OC4ME</sup> which we use for comparisons in the Results section. AAC/C2RCC products, tailored to optically complex coastal waters, delivered the three IOPs  $a_{pig}^{443}$ ,  $a_{dg}^{443}$ , and  $b_{tot}^{443}$ . Both products assume an infinitely deep, homogeneously mixed water column (Doerffer, 2010; EUMETSAT, 2024).

#### 2.3.1. Product selection

A total of 6372 S3OL2 products were acquired using the EUMETSAT Data Access Client (eumdac). For ensuring the highest available data quality level as of June 14, 2024, we acquired both reprocessed (01.01.2018–28.04.2021) and non-time-critical (29.04.2021–31.12.2023) products. Data covered the full Danish EEZ and spatial working grid, bounded by 3–17°E and 54–59°N.

In addition, we downloaded all available products matching dates and locations in the *in situ* dataset for matchup analyses with S3OL2 data

(Bracher et al., 2025a; Bracher et al., 2025b).

#### 2.3.2. Data processing

Data handling was performed in R (v4.2.1), using the 'terra' package (v1.8-15) for spatial processing. From both S3OL2-BAC and AAC products, relevant variables (CHL\_OC4ME, CHL\_OC4ME\_err, CHL\_NN, CHL\_NN\_err, ADG443\_NN, TSM\_NN) were extracted from NetCDF files. Only pixels with chlorophyll values exceeding their respective uncertainty estimates were retained, and datasets were masked using WQSF flags ('INVALID', 'CLOUD', 'SNOW\_ICE', 'SUSPECT', 'HISOLZEN', 'SATURATED', 'HIGHGLINT', 'CLOUD\_AMBIGUOUS', 'CLOUD\_MARGIN', 'OCNN\_FAIL') to exclude unreliable observations. Remaining data were transformed into spatial point vectors, reprojected, and rasterized onto the 500 × 500 m grid using daily log-transformed mean values. Each variable was exported as GeoTIFFs and daily mean composites were generated.

#### 2.3.3. Multivariate outlier removal

S3OL2 C2RCC products can contain unrealistic spectra/combinations between IOPs, which have been omitted in training the C2RCC neural network (Doerffer, 2010). Hence, we applied the multivariate outlier identification method described in Holbach et al. (2025). This method is based on "the minimum covariance determinant (MCD) estimator for robust estimates of the means of and the covariance matrix between the three variables on log-scale" (Holbach et al., 2025) and derived from ISO 16269-4. Corresponding means and covariance matrix for the IOPs were re-used from Table 1 in Holbach et al. (2025). All sets with corresponding Mahalanobis distance >97.5 percentile of a chi-squared distribution with 3 degrees of freedom were excluded.

#### 2.3.4. IOP retrieval

To derive the original  $a_{pig}^{443}$ , Eq. (1) was rearranged into:

$$a_{pig}^{443} = \left( \frac{Chla}{Chl_{fact}} \right)^{Chl_{exp}^{-1}} \quad (2)$$

While  $Chl_{exp}$  and  $Chl_{fact}$  are set to the S3OL2 products defaults of 1.04 and 21, respectively (Section 1). Key assumption (1) (see Section 1) that

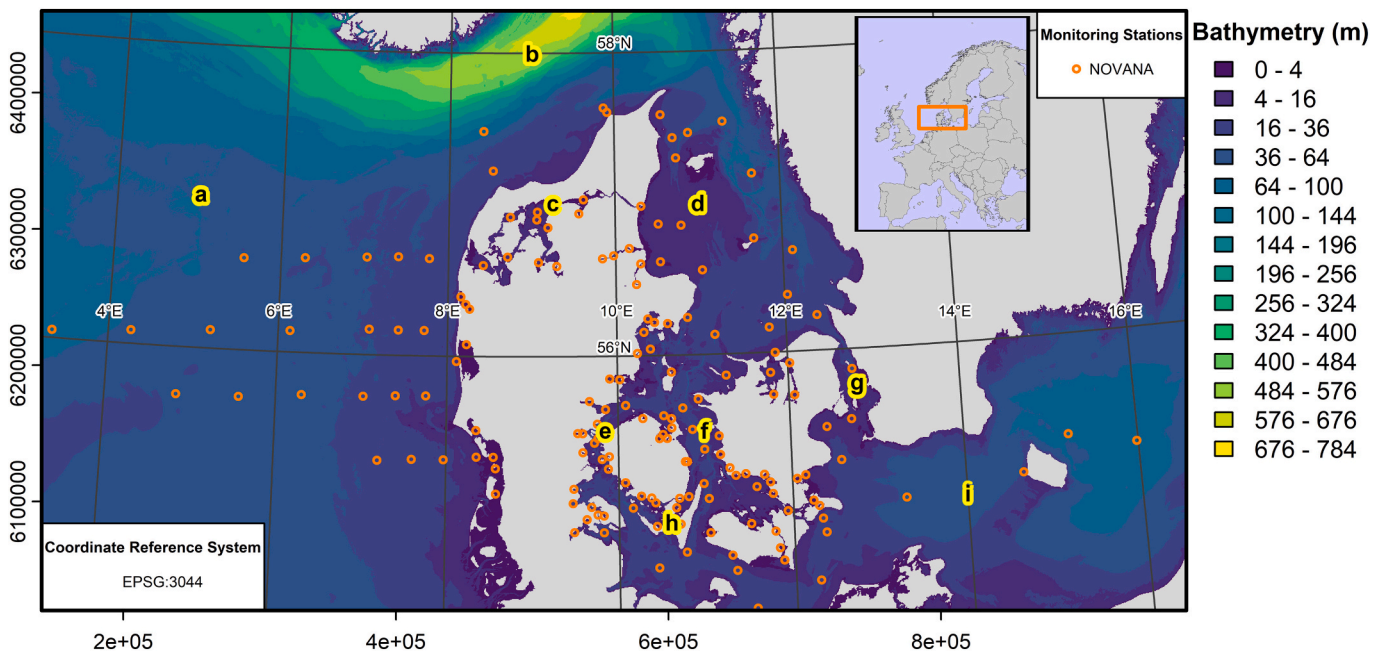


**Fig. 1.** Study area, bathymetry and 163 *in situ* monitoring stations (denoted by orange circles) for marine *Chla* across the Danish Seas. Highlighted letters indicate the following marine regions used for reference in the text: a: North Sea, b: Skagerrak, c: Limfjord, d: Kattegat, e: Little Belt, f: Great Belt, g: The Sound, h: South Funen Archipelago, i: Arkona Basin.



C2RCC reliably derives values for  $a_{pig}^{443}$  was tested through correlation analysis with the independent global reference dataset (Bracher et al., 2025a; Bracher et al., 2025b).

## 2.4. Deviation analysis and masking of matchup pairs

S3OL2 C2RCC products are sensitive to optically shallow waters and low solar zenith angles. We have excluded all daily matchups from the months November to February from the following analyses (Holbach et al., 2025; Staehr et al., 2023). Based on a spectral and S3OL2 based method (Holbach et al., 2025), we derived a data layer for 25th-percentile of diffuse light attenuation coefficient  $K_d^{PAR}$ . The unitless product of light attenuation coefficient  $K_d^{PAR}$  and water depth  $z$  ( $\tau = K_d^{PAR} \times z$ ) is called ‘optical depth’  $\tau$  and depicts possible influence of reflectance from sediment on remote sensing reflectance. We tested if derived optical depth and bathymetry classes had an impact on the magnitude of deviation between *in situ*  $Chla$  and the original S3OL2  $CHL_{NN}$  for all available day-precise matchups. From this analysis, we intended to identify meaningful thresholds for optically too shallow waters and for the efficient masking of  $Chla$  related S3OL2 data.

## 2.5. Geographically weighted regression modelling

### 2.5.1. Background

Geographically weighted regression (GWR) modelling (Charlton and Fotheringham, 2009) is used in marine remote sensing studies to account for non-stationary relationships between variables (Gholizadeh and Robeson, 2016; Nazeer and Bilal, 2018). Gholizadeh and Robeson (2016) for example described the non-stationary relationship of specific  $Chla$  absorption and  $Chla$  concentrations on large spatial scale. Instead of a single regression function from an x-y scatterplot, each point in space will receive its own regression function based on spatial distance-based weighting of x-y pairs. While Euclidean distances are mostly applied in GWR, it is possible and intended to apply other distance measures, when it makes sense (Charlton and Fotheringham, 2009).

### 2.5.2. In-water cost-distance approach

In this study, GWR was used to examine the spatially varying relationship between  $a_{pig}^{443}$  and  $Chla$  in a complex near-coastal marine environment. We considered Euclidean distance not suitable for complex coastlines, as this can lead to problematic assignments of weights (see suppl. Information and suppl. Figs. S1–4 for clarification). To account for the influence of shoreline complexity and bathymetric variation on hydrological connectivity, we developed an in-water cost-distance approach. Cost-distances should describe realistic hydrological connectivity, assigning higher cost-distance to points only connected by narrow and/or shallow passages and lower cost-distance to points connected by offshore deep water.

Cost-distances were calculated using the raster-based costDist() function from the R-library ‘terra’. Raster cells may be passed in eight directions, while a friction layer’s value for the cell is multiplied with the real spatial distance of the cell-passage. Cost-distance between two points is then assigned to the minimum sum of cell-passage costs selected from all possible connection paths. Here, we used a two-step approach:

- We computed the cost-distance from all water pixels to shoreline using bathymetry as the friction layer. This estimates the minimum integrated bathymetric proximity (IBP) (Holbach et al., 2025) of a certain point to the shoreline, representing the minimum cross-sectional area through the water column from the point to the shore.
- The resulting IBP surface was then reciprocally transformed to generate the actual hydrological friction layer  $f$  used to calculate inter-point connectivity.

$$f = 1 + \frac{p_{cost}}{\sqrt{IBP}} \quad (3)$$

Here,  $p_{cost}$  is a cost-parameter that equals an arbitrary value of  $\sqrt{IBP}$ , where  $f = 2$ . We tested three scenarios for  $p_{cost}$  and set it to 0, 1000, and 10,000, respectively. Theoretically, a pixel infinitely deep or far away from the coast will receive  $f \approx 1$ , hence cost-distance when passing the pixel will almost equal real distance. For  $p_{cost} = 0$ , friction  $f = 1$  and cost-distances will equal in-water distances, where all passages through water pixels are equally allowed. For  $p_{cost} = 1000$ , a point 10 km away from the coast at a constant depth of 10 m will in contrast receive  $f = 11$ , hence cost-distance when passing the pixel will be 11 times real distances. Points on land ( $IBP = 0$ ) will receive  $f = \infty$  and cannot be passed. This transformation prioritizes deeper, more open-water pathways, aligning with realistic routes of biological, or hydrodynamic interaction. Two points from hydrologically separated water bodies, e.g. by narrow and shallow passages (see Limfjord (c), or Little Belt (e) in Fig. 1) will get assigned much larger cost-distances than points from within the same hydrological water body. When used within the GWR framework, spatial weighting reflects not just geographic proximity, but also the underlying hydrological structure affecting environmental gradients and relationships between  $a_{pig}^{443}$  and  $Chla$ .

### 2.5.3. Weighted linear regression modelling

For GWR calculations, we used the logarithmic form of Eq. (1):

$$\log(Chla) = \log(a_{pig}^{443}) \times Chl_{exp} + \log(Chl_{fact}) \quad (4)$$

Consequently,  $Chl_{exp}$  equals the slope and  $\log(Chl_{fact})$  the intercept of a linear regression function between  $\log(Chla)$  and  $\log(a_{pig}^{443})$ . The x-y pairs to feed into the GWR procedure, were derived from day-precise matchups between *in situ*  $Chla$  monitoring and S3OL2 based estimates of  $a_{pig}^{443}$ . We calculated a point-to-point cost-distance matrix between all these matchups. Then we used this distance matrix to approximate  $Chl_{exp}$  and  $Chl_{fact}$  for the linear regression function of each monitoring station. We applied cost-distance weighted geometric mean regression by using the bfls() function from R-library ‘bfls’ (v0.2.0). Geometric mean regression assumes uncertainty for both variables. This makes sense here as both the *in situ*  $Chla$  samples and satellite records of  $a_{pig}^{443}$  represent proxies for daily surface  $Chla$  concentrations, each having associated uncertainty.

The bfls() method allows for assigning weights to each data point. For the calculation of weights, we applied a Gaussian kernel (Charlton and Fotheringham, 2009) on the point-to-point cost-distances  $d_{ij}$ :

$$w_{ij} = \exp\left(-3 \times \left(\frac{d_{ij}}{h}\right)^2\right) \quad (5)$$

Here,

- $w_{ij}$  is the weight of point  $j$  for the regression at point  $i$ ,
- $d_{ij}$  is the cost-distance between points  $j$  and  $i$ ,
- $h$  is a measure for the width of the Gaussian kernel where  $w_{ij} \approx 0.05$ , here we set it to the median point-to-point cost-distance between NOVANA stations.

Within the bfls() function, weighting is done based on assigned uncertainty. In the case of geometric mean regression, this uncertainty equals the standard deviation of the corresponding variable. For weighted geometric mean regression between  $Chla$  and  $a_{pig}^{443}$  as variables  $v$ , we therefore based the uncertainty assigned to a matchup pair between points  $i$  and  $j$  on the standard deviation of each input variable  $\sigma(v)$  and the respective cost-distance weights  $w_{ij}$  according to York (1968) and the documentation of the bfls() function:



$$\sigma_{ij}(v) = \frac{\sigma(v)}{\sqrt{w_{ij}}} \quad (6)$$

Now, all the elements for GWR modelling of the linear regression function in Eq. (4) have been defined, and `bfs()` can be applied for each monitoring station to estimate  $Chl_{exp}$  and  $Chl_{fact}$ . An exemplary R-code for reproducing the method is provided in the suppl. Information.

To limit the GWR models to matchup pairs with significant influence and to avoid GWR modelling for stations without close connection to valid matchup data, we set two additional quality restrictions in the GWR modelling:

- The daily matchup pairs used for GWR modelling of a target station were limited to those stations, where the 200 matchup pairs with least cost-distance to the target station derived from.
- GWR modelling was only calculated for stations, where there were at least five nearby matchup pairs with  $w_{ij} > 1/3$

## 2.6. Validation and calibration

We assume that C2RCC derives reliable values for  $a_{pig}^{443}$ , and that the scaling factors  $Chl_{exp}$  and  $Chl_{fact}$  can be approximated by a purely spatial approach (see Section 1). Consequently, GWR modelling for the same station should deliver comparable linear relationships between *in situ*  $Chla$  and C2RCC based  $a_{pig}^{443}$ , independent of the period used. To validate the GWR modelling approach, we therefore split our day-precise matchup dataset temporally into two equal time periods, from 2018 to 2020 (p1) and 2021–2023 (p2). As a form of cross-validation, we then applied the derived scaling factors  $Chl_{exp}$  and  $Chl_{fact}$  from p1 on  $a_{pig}^{443}$  from p2 (Eq. (4)), and *vice versa*, in order to derive S3OL2 based estimates of  $Chla$ . Hence, we applied totally independent matchup datasets both for calibration and validation of GWR models. We tested three scenarios for  $p_{cost}$  in Eq. (3), and chose the final value according to validation performance metrics. We also tested the same approach for the S3OL2-BAC product  $CHL_{OC4ME}$  and its relationship with *in situ*  $Chla$ .

If successful, we will see significant improvement in the relationship between *in situ* and S3OL2-based  $Chla$  estimations. In this case, we will

use the full matchup dataset to calibrate optimally informed scaling factors  $Chl_{exp}$  and  $Chl_{fact}$  for the monitoring stations.

## 3. Results

### 3.1. In situ surface chlorophyll-a concentration

99 % of the 10,320 daily  $Chla$  values retrieved from 163 NOVANA stations range in-between 0.38 and 65  $\mu g \times L^{-1}$ . 7226 surface  $Chla$  were sampled in the valid months for S3OL2 data in Danish latitudes (Holbach et al., 2025; Staehr et al., 2023) between March to October (Fig. 2). Distributed across 163 stations and 6 years, this leaves on average 0.9 samples per station and month, ranging between a minimum of 0.7 in April and maximum of 1.1 in August.

### 3.2. Satellite-based $CHL_{NN}$

In total, we retrieved 55,722  $CHL_{NN}$  concentrations for the 163 NOVANA stations for surface  $Chla$  monitoring. Multivariate outlier removal on these data, as described in our previous study (Holbach et al., 2025), left 46,761 values, and masking for the valid months for S3OL2 data in Danish latitudes (Holbach et al., 2025; Staehr et al., 2023) between March to October left 45,170 values for further analysis (suppl. Fig. S5). As described in Section 2.4, we tested if optical depth and bathymetry impacted the magnitude of deviation between *in situ*  $Chla$  and the original S3OL2  $CHL_{NN}$  for all available day-precise matchups (Fig. 3). Based on this analysis, we empirically defined thresholds at  $\tau = 1.5$  optical depths and a water depth of 3.5 m, above which the initial deviations decline drastically, and median deviations remain within a range of 0.5 to 2 times of *in situ*  $Chla$  (Fig. 3). The optical depth threshold equals the one that we already identified in our previous study on light attenuation (Holbach et al., 2025).

Masking for these thresholds left 41,973 values from 105 stations. Distributed across 8 months and 6 years, this leaves on average 8.3 S3OL2-based values per station and month, ranging between a minimum of 4.8 in October and maximum of 11.5 in April. S3OL2-based C2RCC products thus deliver valuable information for considerably less stations

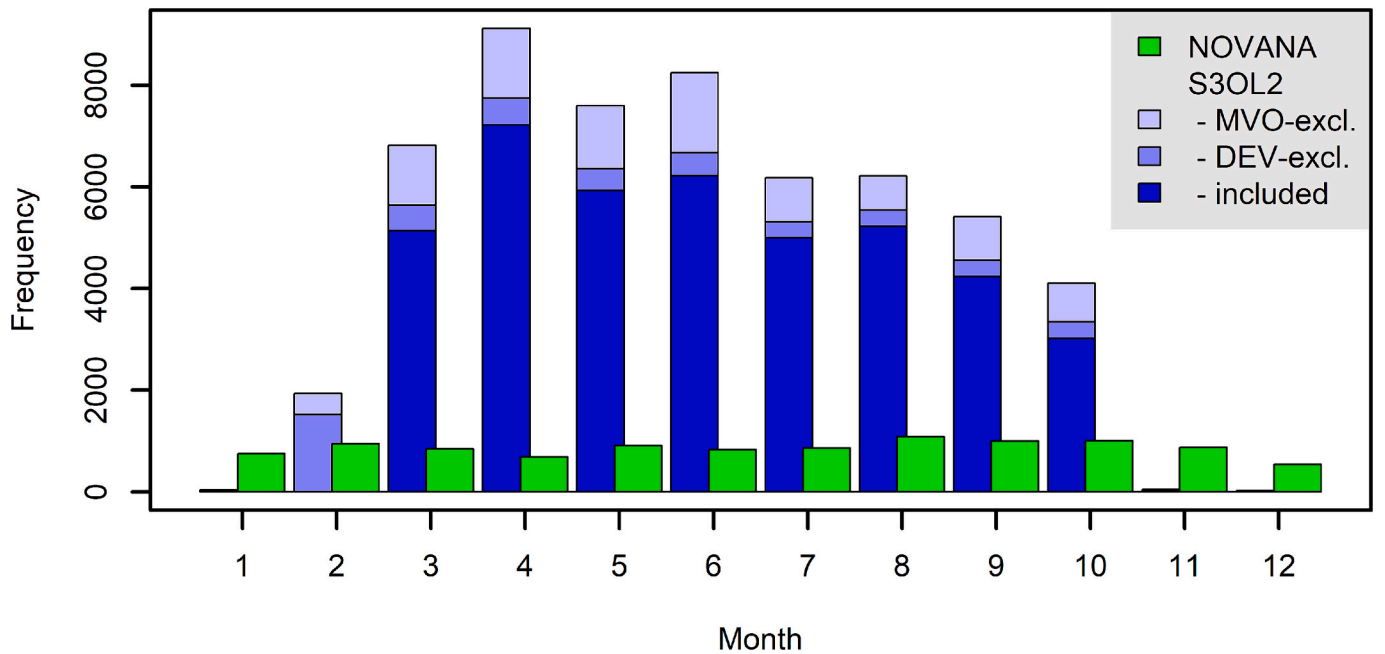
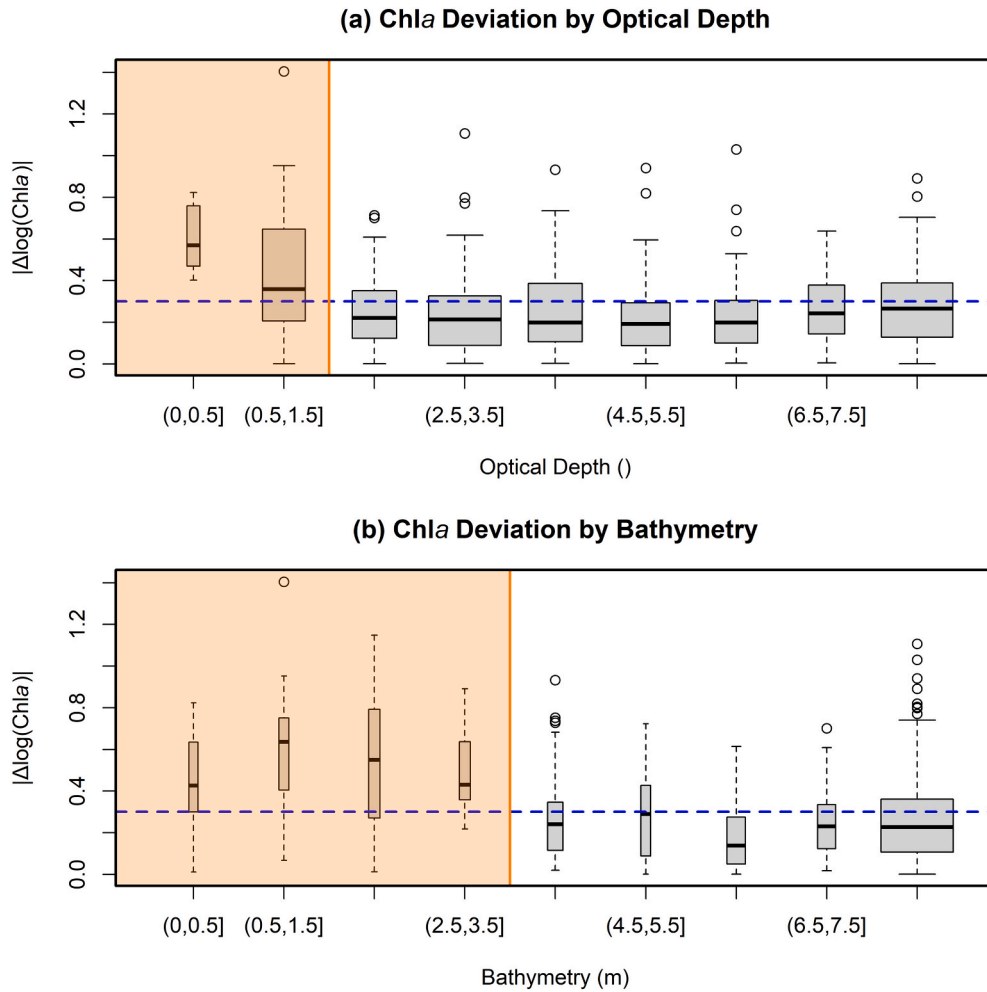


Fig. 2. Temporal distribution of frequencies of  $Chla$  records from both *in situ* measurements in the NOVANA programme (green) and S3OL2 C2RCC products for all analyzed 163 stations. The light-blue parts of bars for S3OL2 represent values excluded from further analysis due to either multivariate outlier detection (MVO-excl.), or due to month, bathymetry, and optical depth- related deviation analysis (DEV-excl.).



**Fig. 3.** Deviation analysis between day-precise matchups of both S3OL2 and *in situ* based *Chla* estimations. Deviations are shown as boxplots of absolute differences on the log-scale for (a) optical depth (0.25-quantile) classes and (b) classification by bathymetry. Dashed blue lines mark a deviation by a factor of either 0.5 or 2 on normal scale. We excluded classes where most of deviations fell above this threshold (orange areas).

and a limited time period from March to October, but for the rest of the stations and times, we could receive *ca.* 10 times higher monitoring frequency than from NOVANA.

### 3.3. Matchup analysis and geographically weighted regression modelling

Matchup analysis between the global reference data on *in situ* spectral phytoplankton absorption coefficients at 442.5 nm (Bracher et al., 2025b) and correspondingly processed daily C2RCC-based  $a_{pig}^{443}$  resulted in 326 valid matchups, a Pearson's  $R = 0.76$ , and a distribution of points along the 1:1 line (suppl. Fig. S6). Consequently, we can assume a valid C2RCC-based estimation of  $a_{pig}^{443}$  and can use  $R = 0.76$  as benchmark for the best possible result in corresponding *Chla* estimation.

For our study area and after masking, we obtained a total of 987 day-precise matchups between *in situ* *Chla* and satellite-derived  $a_{pig}^{443}$ , almost evenly distributed across the two validation periods (2018–2020: 451; 2021–2023: 536). C2RCC-based  $a_{pig}^{443}$  showed a moderately strong Pearson's correlation with *in situ* *Chla* ( $R = 0.59$ ; Fig. 4 (a)). Across the study area, S3OL2-AAC CHL\_NN slightly overestimated *in situ* *Chla* with a mean bias error (MBE) of 0.15 on the log-scale, and a Root Mean Square Error (RMSE) of 0.3. A global matchup calibration by geometric mean regression on the log-scale, resulted in  $Chl_{exp}^{glob} = 1.37$  and  $\log(Chl_{fact}^{glob}) = 1.48$ , an MBE of 0 (as expected due to calibration with the same data) and RMSE of 0.29.

In contrast, the S3OL2-BAC product (CHL\_OC4ME) for open ocean conditions showed a weaker correlation ( $R = 0.4$ ) and notably higher error metrics ( $RMSE = 0.69$ ;  $MBE = 0.54$ ; suppl. Fig. S7). These results already clearly indicate that the S3OL2-AAC products are better suited than S3OL2-BAC products to estimate surface *Chla* in optically complex waters.

#### 3.3.1. Validation

After splitting up the data into two equally long time periods, we calculated GWR models for each period, each monitoring station, and each of the three  $p_{cost}$  scenarios. The process is visualized by the orange (2018–2020) and blue (2021–2023) clusters of regression lines in Fig. 4 for  $p_{cost} = 1000$ . After the GWR models were applied to matchup-pairs from the respective other reference period, Pearson's  $R$  between S3OL2- and *in situ*-based *Chla* reached 0.6536, 0.6542, and 0.6516 for the three  $p_{cost}$  scenarios respectively. MBE was almost zero (Fig. 4 (b)) in all cases. Hence, we decided to continue with  $p_{cost} = 1000$  due to the slightly better correlation. The resulting station-specific scaling factors  $Chl_{exp}$  and  $\log(Chl_{fact})$  correlated between the two periods with Pearson's  $R$  values of 0.61 and 0.34, respectively. The ranges of estimated values of scaling factors were:  $0.80 \leq Chl_{exp} \leq 2.97$  (default 1.04), and  $1.12 \leq \log(Chl_{fact}) \leq 2.71$  (default  $\log(21) = 1.32$ ).

At the same time, RMSE was reduced from 0.29 to 0.27. These results show that regionalized relationships between  $a_{pig}^{443}$  and *in situ* *Chla* modelled through the developed GWR approach can be used to estimate

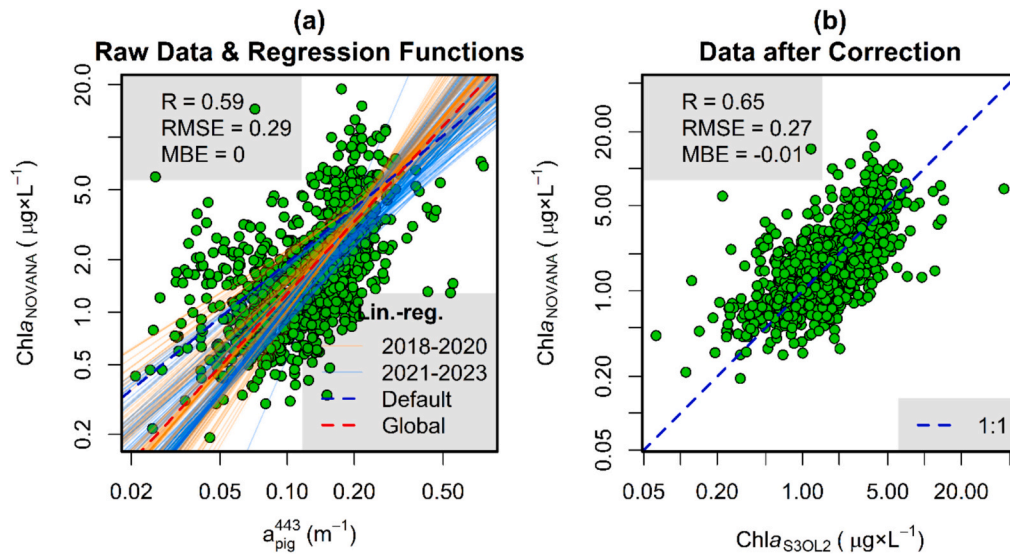


**Fig. 4.** Validation of the spatially weighted linear regression modelling approach for S3OL2 based surface *Chla* estimation. (a) Correction for day precise matchup pairs from 2018 to 2020 is done based on station specific linear regression functions calculated on matchup pairs from 2021 to 2023, and the other way round. The scatterplot of all day precise matchup pairs between  $a_{pig}^{443}$  and *in situ* *Chla* (green points) is overlaid with station specific regression lines for the two periods 2018–2020 (light orange) and 2021–2023 (light blue). The default linear translation function used in S3OL2 products is shown as dashed dark blue line. (b) Scatterplot of all matchup pairs after application of the station specific linear regression functions to translate  $a_{pig}^{443}$  to S3OL2 based *Chla*. Person's *R*, root mean squared error (RMSE) and mean bias error (MBE) statistics are shown for the default linear regression function in (a) and the station specific linear regression correction in (b). Remark: statistics are calculated on the log-scale and in (a) RMSE and MBE refer to the default CHL\_NN S3OL2 products.

spatially variable scaling factors  $Chl_{exp}$  and  $Chl_{fact}$ , that empirically translate  $a_{pig}^{443}$  into *Chla*. Our validation experiment has shown that these significantly improve the agreement between surface *Chla* estimates from S3OL2-based C2RCC products and *in situ* samples, even when applied on temporally independent matchup datasets.

For comparison, we applied the same validation procedure on the S3OL2-BAC product CHL\_OC4ME (suppl. Fig. S7). The results showed

very chaotic clusters of local regression lines and application of GWR models to the matchup-pairs from the respective other reference period failed to improve performance, opposition fact, the fit worsened. This indicates that the approach is not suitable for CHL\_OC4ME.

### 3.3.2. Calibration

After successful validation, we applied the developed GWR proced-

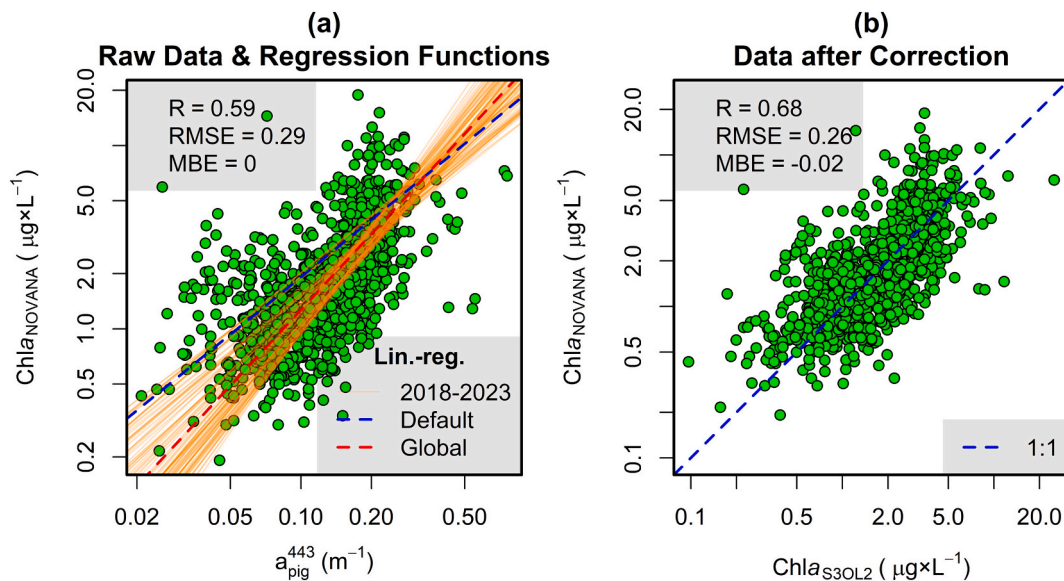


**Fig. 5.** Calibration of the spatially weighted linear regression modelling approach for S3OL2 based surface *Chla* estimation. (a) Correction for day precise matchup pairs is done based on station specific linear regression functions calculated on matchup pairs from the entire study period 2018–2023. The scatterplot of all day precise matchup pairs between  $a_{pig}^{443}$  and *in situ* *Chla* (green points) is overlaid with station specific regression lines (light orange). The default linear translation function used in S3OL2 products is shown as dashed dark blue line. (b) Scatterplot of all matchup pairs after application of the station specific linear regression functions to translate  $a_{pig}^{443}$  to S3OL2 based *Chla*. Person's *R*, root mean squared error (RMSE) and mean bias error (MBE) statistics are shown for the default regression function in (a) and the station specific linear regression correction in (b). Remark: statistics are calculated on the log-scale and in (a) RMSE and MBE refer to the default CHL\_NN S3OL2 products.



ure on the entire dataset of 987 day-precise matchups from the time period from 2018 to 2023 to retrieve an optimally informed calibration of the relationship between S3OL2 C2RCC-based  $a_{pig}^{443}$  and *in situ* *Chla* for each station (Fig. 5). Ranges of the estimated scaling factors got slightly more narrow:  $0.93 \leq Chl_{exp} \leq 2.19$  (default 1.04), and  $1.24 \leq \log(Chl_{fact}) \leq 2.15$  (default  $\log(21) = 1.32$ ).

After the resulting GWR models were applied to all matchup-pairs, Pearson correlation between S3OL2- and *in situ*-based *Chla* reached  $R = 0.68$ , MBE remained at almost zero, and RMSE reached 0.26 (Fig. 5 (b)).

For clarity, we selected eleven monitoring stations from throughout the study area, to visualize the specific calibration procedure in more detail (Fig. 6 and suppl. Figs. S8–S18). The chosen stations are marked by numbers 1–11 in the maps in Fig. 7 and Fig. 8. Parts (a) of these figures show the weighted linear regression on the background of the entire matchup scatterplot. Point sizes depict assigned weights and points with black boundaries are those used for GWR ( $n \geq 200$ ) according to the criteria described in Section 2.5. Points with orange boundaries are matchups derived directly from the target station. Parts (b) of these Figures show the corresponding spatial context, where point sizes indicate similarly the weights assigned to each station. Again, only stations with black boundaries are used to support the GWR model in addition to the target station itself (orange boundary).

#### 3.4. NOVANA station time-series

Beyond the 987 day-precise matchup pairs, both *in situ* and S3OL2 datasets contained substantially larger volumes of data. To support the validity of GWR based method, there should also be good agreement of overall temporal trends between both datasets. Therefore, we visualized time-series data for the eleven selected stations across the entire study area in parts (c) of Fig. 6 and suppl. Figs. S8–S18, offering qualitative insight into temporal variability at the monitoring station level.

Overall, we observed good agreement of the magnitude and temporal trends in time-series from all stations. However, phytoplankton blooms in early spring and late autumn get well captured by *in situ* *Chla* data but get missed by S3OL2-based *Chla*. This can be seen for example at station no. 2 (suppl. Fig. S9), where elevated surface *Chla* (up to  $70 \mu\text{g} \times \text{L}^{-1}$ ) persisted from late 2019 throughout the winter. A similar pattern is evident in station no. 4 (suppl. Fig. S11), where highest concentrations often occur during winter months clearly observed through *in situ*, but unseen by S3OL2-based *Chla*.

#### 3.5. Spatially continuous satellite-based *Chla* monitoring

A key advantage of satellite-based imagery over traditional ship-based sampling is its ability to provide spatially continuous observations of environmental phenomena (Strong and Elliott, 2017; Toming

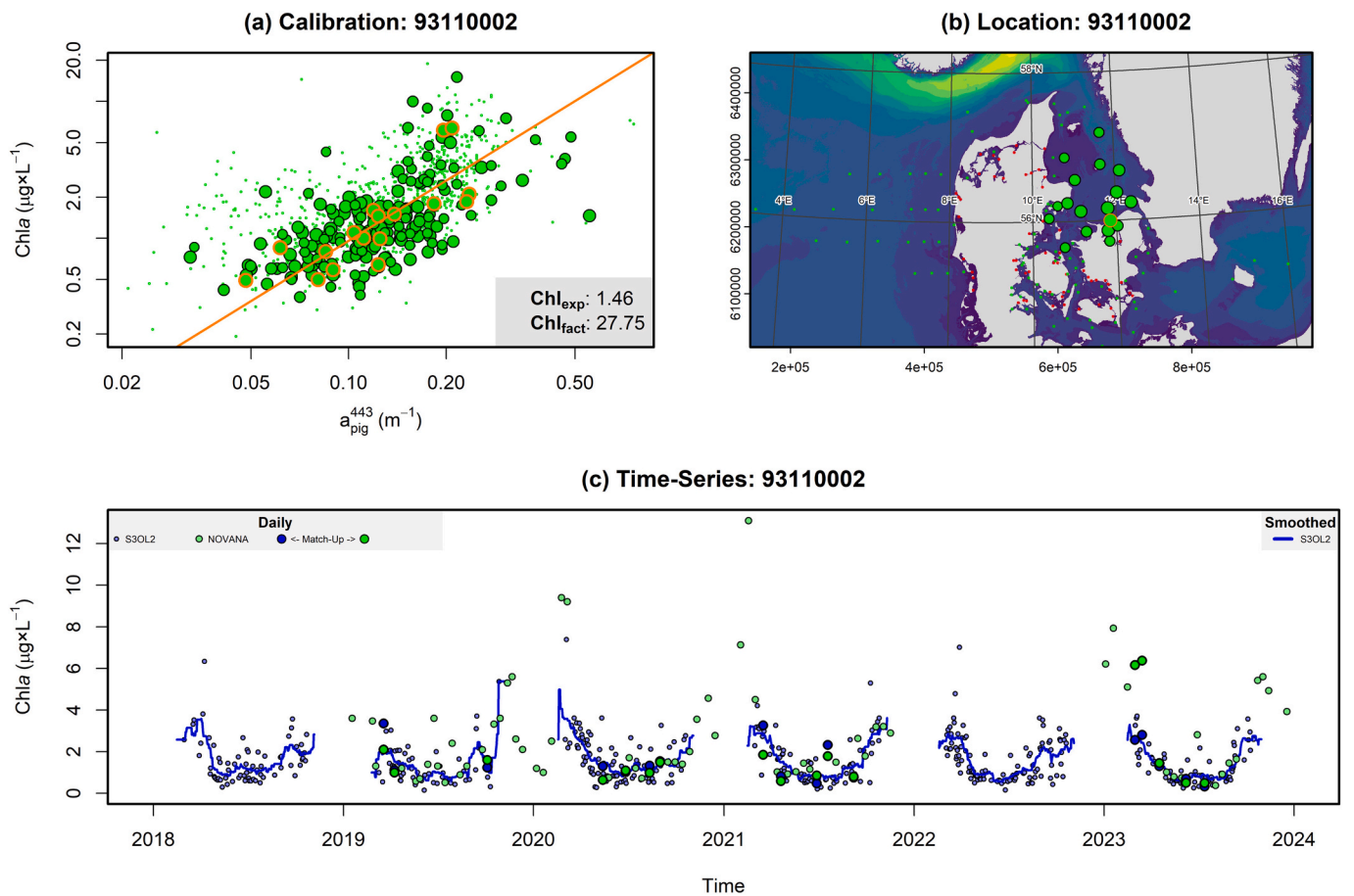


**Fig. 6.** Example of the spatially weighted calibration procedure and derived time-series overlay between S3OL2 and *in situ* based *Chla* for NOVANA station 93,110,002 (see number 6 in Fig. 7 and Fig. 8). (a) Scatterplot of day precise matchups between S3OL2 based  $a_{pig}^{443}$  and *in situ* surface ( $\leq 1$  m) *Chla* concentration. Highlighted points and sizes represent weights for spatially weighted station specific regression calculations. The derived local regression function for this station is shown as orange line and estimates of the two derived scaling factors are given in the legend. (b) Spatial representation of the weights of different monitoring stations, NOVANA station 93,110,002 is highlighted with an orange boundary. (c) Time-series for NOVANA station 93,110,002 from 2018 to 2023, overlaying both S3OL2 (blue) and *in situ* (green) based estimates of surface *Chla* concentrations. Day precise matchup pairs are highlighted by larger points. For S3OL2, a  $\pm 15$  days moving average is also shown (dark blue line). Remark: Similar graphs for the remaining numbered points in Fig. 7 and Fig. 8 are provided in suppl. Figs. S8–S18.

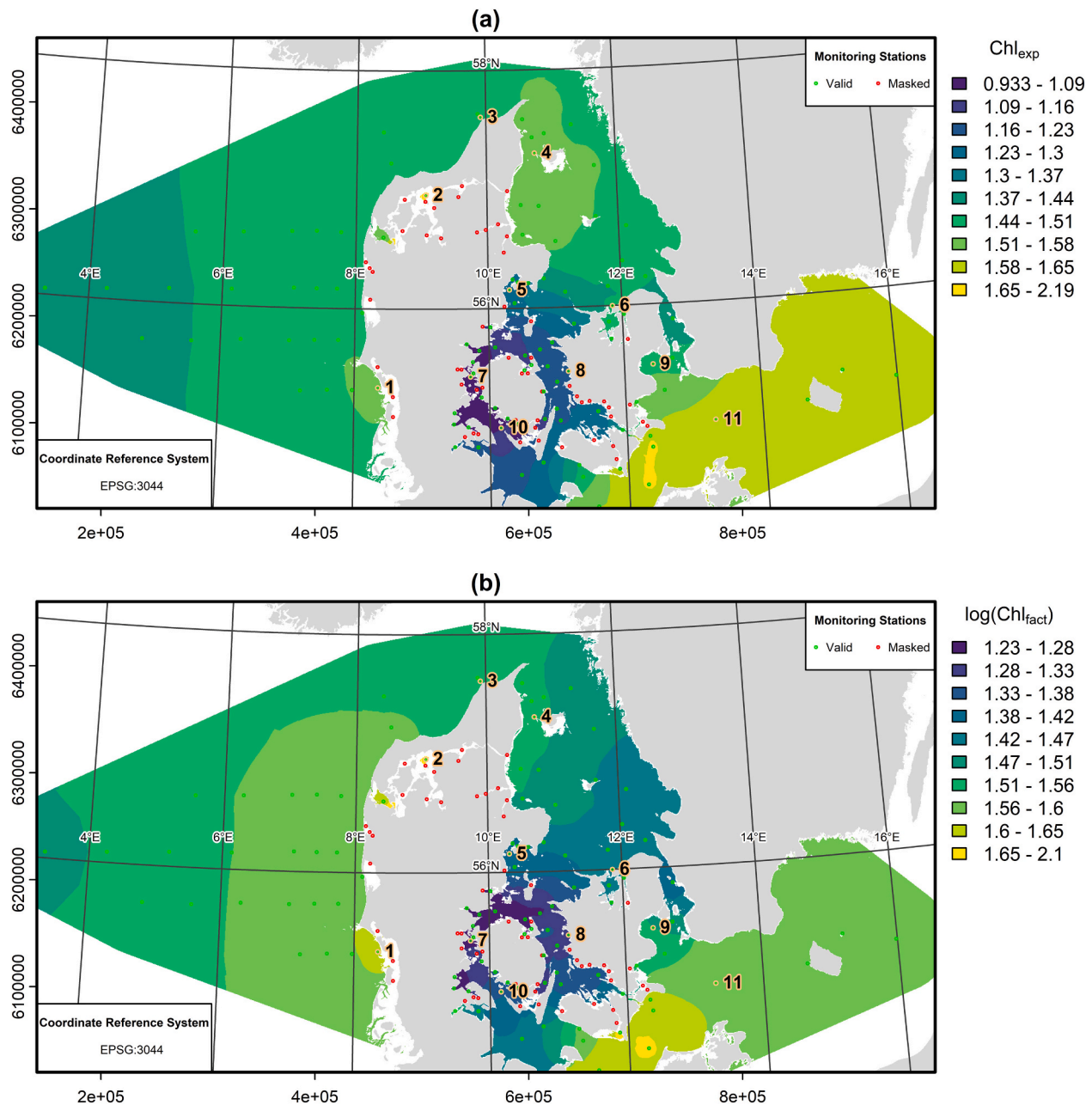


**Fig. 7.** Spatially interpolated models of the two scaling factors (a)  $Chl_{exp}$  and (b)  $Chl_{fact}$  used to translate  $a_{pig}^{443}$  into S3OL2  $Chla$  according to Eq. (1). White areas are masked out due to either optical depth  $< 1.5$ , bathymetry  $< 3.5$  m, or the convex hull with 50 km buffer around valid calibration stations. The 105 monitoring stations used for calibration are shown in green, while masked monitoring stations are shown in red. The highlighted numbers and points refer to stations explicitly analyzed in Fig. 6 and suppl. Figs. S8-S18.

et al., 2017). Until now, our analysis has focused on satellite-derived data at individual monitoring stations.

To generate continuous spatial layers of these scaling factors, we applied an advanced kriging interpolation procedure tailored for complex coastlines. This method leverages the same cost-distance used for the GWR modelling, to derive smooth and continuous spatial distribution data layers of the two scaling factors (Fig. 7). Instead of Euclidean distances, the kriging interpolation is based on a stack of cost-distance surfaces for each point. It takes a fitted power variogram model and performance is checked with leave-one-out cross-validation. Results comprise both the interpolated surface of the target variable and an associated kriging uncertainty. This specific interpolation procedure is a tool developed in-house. A full description of this tool is beyond the scope of this paper. Detailed information can be obtained from the

corresponding author.

To avoid extensive extrapolation into areas without ground truthing, we constrained the interpolation at an arbitrary distance of 50 km from a convex hull around all monitoring stations with matchup data. The resulting interpolated layers of the scaling factors exhibit similar spatial patterns across the study area with lowest values surrounding the island of Funen including the areas Little Belt (e), Great Belt (f), and South Funen Archipelago (h), previously outlined in Fig. 1. The highest values were observed within Limfjord (c).

Corresponding maps of kriging uncertainty for  $Chl_{exp}$  and  $\log(Chl_{fact})$  are provided in suppl. Fig. S19. These uncertainties are very small (mostly  $< 0.05$ ) compared to the variation range of the two scaling factors. Thus the 50 km extrapolation buffer is well justified.

The spatially continuous models of scaling factors can then be

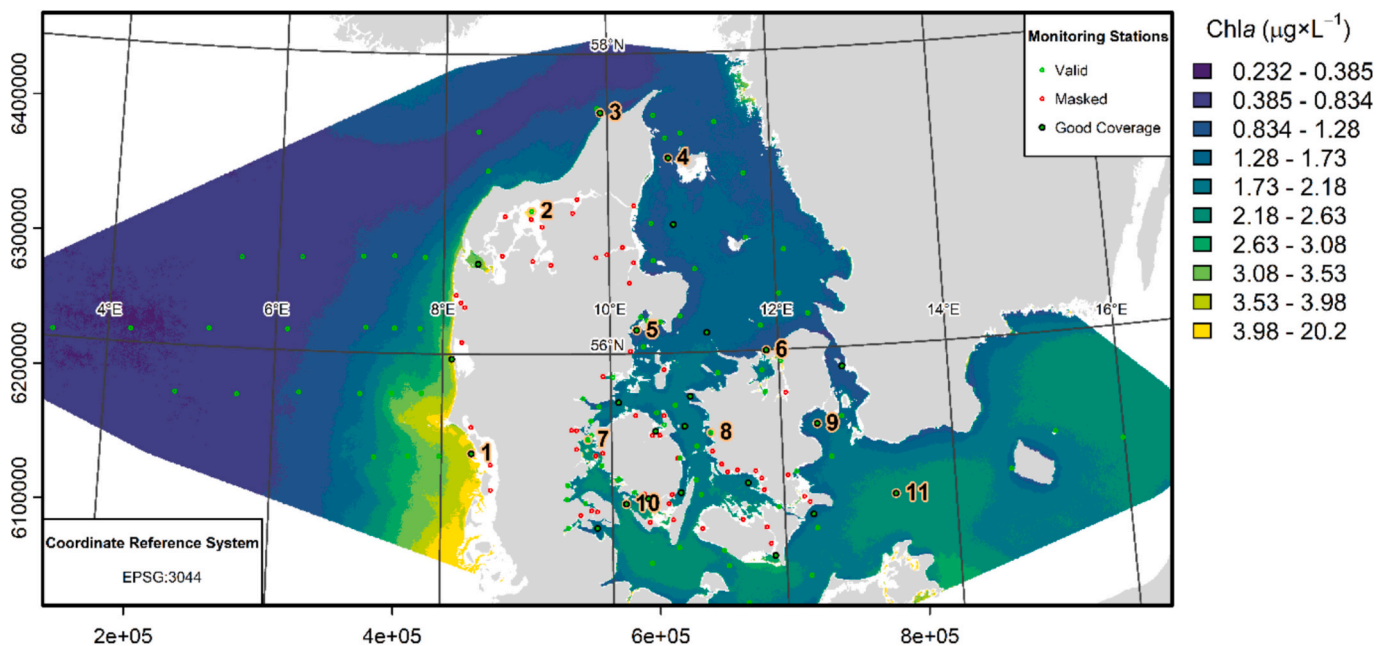


**Fig. 8.** Map of median surface  $Chla$  based on S3OL2 products and the developed spatial correction model for the years 2018–2023. The 105 valid monitoring stations used for calibration are shown in green, while masked monitoring stations are shown in red. 23 stations with good coverage from both *in situ* and S3OL2 data are marked by a black circle and used in Section 3.6. The highlighted numbers and points refer to stations explicitly analyzed in Fig. 6 and suppl. Figs. S8-S18.

applied on S3OL2 C2RCC-derived  $a_{pig}^{443}$  images to derive images of  $Chla$  estimates. As an example, we calculated median  $Chla$  for each pixel and the entire period from 2018 to 2023 (Fig. 8). In principle, however, it is possible to derive daily maps of satellite-based  $Chla$ . Blank areas in the map are those masked out due to optically shallow waters or due to being out of the spatial scope area of ground truthing points.

Distinct spatial patterns emerge from the derived S3OL2-based  $Chla$ , with notably high concentrations close to and along the Danish west coast. A clear gradient is also evident, showing increasing  $Chla$  values from the open North Sea (a) through Skagerrak (c), Kattegat (d), the belt sea (e-g), and into the Baltic Sea with the Arkona Basin (i) (see Fig. 1 for place names). Further, we show a map of the difference between the global calibration with constant scaling factors (see Section 3.3) and optimized median  $Chla$  (Fig. 8) in suppl. Fig. S20.

### 3.6. Long-term assessments

For ecological assessments, data are long-term aggregated, such as for the 6-year reporting periods of  $Chla$  concentrations in the EU water framework directive (EU, 2000). Hence, we tested the agreement of aggregated averages for the whole six-year study period from 2018 to 2023. To account for uneven temporal distribution, monthly means were first calculated, followed by annual averages, and finally a multi-year average over the six-year period, all log-scaled. Further, we made a rigorous selection of stations to only include those with good coverage from both datasets across all six years and all 8 months with valid S3OL2 data:

- Only months with at least two *in situ* and four S3OL2  $Chla$  values,
- years with at least 6 months covered,

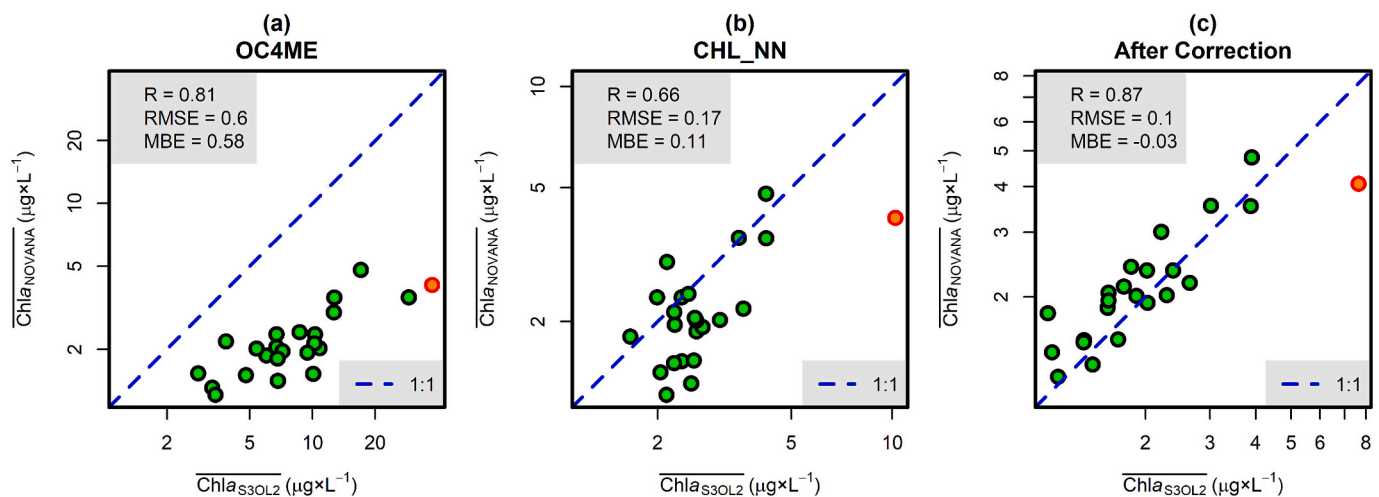


**Fig. 9.** Comparison of long-term (2018–2023) average  $Chla$  from both *in situ* and S3OL2-based observations for 23 monitoring stations with robust temporal coverage from both methods. (a) scatterplot for the S3OL2-BAC product CHL\_OC4ME, (b) scatterplot for the S3OL2-AAC CHL\_NN product, and (c) scatterplot for the GWR corrected product developed in this study. One outlying observation (within Odense Fjord) showed strong overestimation by S3OL2-AAC based observations. This point is marked in orange and was excluded from statistical calculations.



- and stations with at least 4 years covered were considered.

In total, this left 23 stations (marked in Fig. 8) with robust estimates of long-term average *Chla* from both satellite-based and *in situ* methods (Fig. 9). There was a very good agreement between the GWR corrected S3OL2-AAC validation product and *in situ* surface *Chla* close to the 1:1 line ((c) in Fig. 9). One outlying point, representing a station within Odense Fjord, showed a strong overestimation by S3OL2 and was excluded from statistical calculations. Pearson correlation between S3OL2- and *in situ*-based *Chla* reached  $R = 0.87$ , MBE was close to zero but showed a slight underestimation by S3OL2 compared to day-precise matchup analysis, and RMSE reached 0.10 (all calculated on a log-scale). These statistical measures clearly outperformed those from the other two tested S3OL2-based products.

## 4. Discussion

This study demonstrates a novel, spatially explicit and data-driven approach to improving the accuracy of satellite-derived *Chla* estimates in optically complex coastal waters at regional scale. Scaling factors, used in the C2RCC processor to translate IOP estimates for  $a_{\text{pig}}^{443}$  into surface *Chla*, were optimized locally by means of an innovative cost-distance based GWR of day-precise matchups between *in situ* samples and S3OL2 C2RCC based IOP products.

### 4.1. Geographically weighted regression models

Our findings confirm that a fixed set of *Chla*-specific scaling factors, as applied in default S3OL2 C2RCC products, is insufficient to capture the inherent spatial variability in phytoplankton absorption properties in complex coastal settings. Instead of using constant (maybe locally tuned) scaling factors, this study provides the means for spatially dynamic and continuous fields of the *Chla* scaling factors ( $Chl_{\text{exp}}$ ,  $Chl_{\text{fact}}$ ). These spatially resolved scaling factors significantly improved the agreement between satellite-derived and *in situ* *Chla* concentrations, particularly in shallow and estuarine systems where default products typically deliver biased *Chla* levels (e.g. O’Kane et al., 2024; Staehr et al., 2023). Our method captures local hydrological connectivity structures and is considered more suitable for complex coastlines than traditional GWR with Euclidean distances.

Validation results demonstrate that the GWR models notably improve the agreement between S3OL2 C2RCC-derived and *in situ* *Chla* concentrations, even though the subset of matchups used for GWR, was derived from another independent period. The correlation coefficients ( $R = 0.61$  for  $Chl_{\text{exp}}$  and  $R = 0.34$  for  $\log(Chl_{\text{fact}})$ ) between the two time periods (2018–2020 and 2021–2023) indicate a moderate relationship, suggesting that while there is temporal variability, the GWR models can effectively capture systematic regional differences in *Chla*-specific absorption properties. This temporal consistency supports the robustness of the GWR approach at the timescales used within this study from days to up to six years. This way, underlying biogeographical differences in optical water properties are effectively captured. However, the existing temporal variability makes temporal re-calibrations necessary. Chu et al. (2018) have demonstrated significant temporal variations in the relationships between remote sensing reflectance and water quality parameters, underscoring the importance of incorporating temporal dynamics into modelling approaches. This is particularly relevant in times of rapid marine climate change (IPCC, 2019), where we cannot expect the spatial models for scaling factors to be constant in the long-term, as environmental conditions for phytoplankton are also changing.

The calibration process, where all 987 matchups from 2018 to 2023 were included, further constrained the spatially varying scaling factors, resulting in narrower ranges ( $Chl_{\text{exp}}$ : 0.93–2.19;  $\log(Chl_{\text{fact}})$ : 1.24–2.15). This refinement improved the consistency between S3OL2-derived and *in situ* *Chla* estimates even more, as reflected by a stronger Pearson

correlation ( $R = 0.68$ ), near-zero mean bias error (MBE), and a further reduction in root mean square error (RMSE) to 0.26. Hence, this available six years period seems to be the current optimum for spatial calibration of *Chla* scaling factors for the settings in Danish marine waters.

Robust satellite-based estimation of surface *Chla* in complex coastal waters with S3OL2 C2RCC-based products, will always require dense coverage with *in situ* data and continuous recalibration of local scaling factors. Based on this study, we recommend a yearly recalibration of scaling factor spatial models for Danish marine waters with matchup data from the last six years. However, this recommendation might change with time, spatial area of interest and availability of *in situ* monitoring data. Derived changes in the scaling factors over time could become useful proxies to identify hotspot areas of temporal change in phytoplankton ecology.

Overall, the results highlight the potential for regionally tuned models to enhance the accuracy of satellite-based *Chla* estimates, particularly in optically complex coastal zones where standard global algorithms perform poorly. Systematic analyses to further finetune and optimize the spatial approach, in particular with respect to different coverage with *in situ* reference data would make sense. Beyond *Chla*, similar GWR model setups could also improve many other satellite-derived water environmental parameters, where regionally different empirical relationships are expected across complex coastal environments.

In contrast to S3OL2 C2RCC products, the GWR approach was not successful when applied to the S3OL2-BAC product (CHL\_OC4ME), which showed unstable and spatially incoherent regression results and no improvement in relationship between S3OL2 and *in situ* based *Chla*. This outcome highlights a key limitation of CHL\_OC4ME for optically and hydrologically complex waters. Major parts of the uncertainties related to the product are obviously not coupled to spatial differences in phytoplankton features, but rather to the fact that the algorithm does not decompose remote sensing reflectance into contributions from spectrally different IOPs. On the other hand, we showcase that C2RCC actually performs well in this spectral decomposition and derivation of IOPs, as it was already demonstrated in another study on diffuse light attenuation coefficient (Holbach et al., 2025).

### 4.2. Implications for marine monitoring and assessment of ecological state

The spatially continuous models of scaling factors enable the generation of *Chla* maps on various temporal aggregation-scales (daily to multi-year), revealing concentration patterns across the Danish marine waters (Fig. 8). By applying an advanced kriging interpolation method using a cost-distance metric, we generated smoothly varying spatial layers of the calibrated scaling factors. The opportunity for highly resolved spatial and temporal analyses can offer valuable insights into regional *Chla* distribution and dynamics, supporting improved marine monitoring, as well as ecosystem understanding and efficient management. Our findings underscore the importance of regionally tuning C2RCC scaling factors to enhance the reliability of *Chla* estimates from operational ocean color products. Moreover, the presented approach provides a transparent, reproducible, operationally feasible framework, transferable to other regions, satellite sensors, and parameters.

Despite the frequently reported issues with regard to over and/or underestimation of *Chla* based on S3OL2 C2RCC products in complex marine waters (Kratzer and Plowey, 2021; Liu et al., 2021; Staehr et al., 2023; Staehr et al., 2022; Töming et al., 2017), we present an advanced way to derive regionally tuned and almost unbiased *Chla* estimates from daily (Fig. 4) to multi-year (Fig. 9) scales that match very well with *in situ* data. Hence, we argue that satellite-derived *Chla* can be efficiently used to supplement traditional ship-based monitoring, even in optically and hydrologically complex coastal waters. This can increase our understanding of eutrophication processes at unforeseen spatial and temporal scales. Still, we must be aware of potential local mismatches, such as the outlier marked in Fig. 9. Odense Fjord, where this station is

located, is a prominent area for eelgrass, which may impact the remote sensing reflectance and make C2RCC interpret the signal as high *Chla* concentration, instead. We need to be aware that C2RCC assumes an infinitely deep, homogeneously mixed water column (Doerffer, 2010; EUMETSAT, 2024).

Our study results have significant implications for marine ecosystem management and compliance with EU directives on eutrophication assessment; however, practical and operational implementation will require thorough analyses before satellite-based *Chla* can be used as a valid eutrophication indicator. Also, spatial upscaling and international alignment of satellite-based methods should be a future priority.

#### 4.3. Preliminary ecological implications

We assumed that the scaling factors are related to the *Chla*-specific absorption properties of phytoplankton communities, which differ in total *Chla* concentration, species and pigment composition, pigment packaging, and size distribution of phytoplankton cells (Ciotti et al., 2002; Martin, 2014; Stæhr and Markager, 2004; Stæhr et al., 2004). Despite a lack of systematic recent data for a direct alignment with our results, it has been shown in 2012 that the Little Belt region (e) was characterized by highest biomasses and highest fractions of diatoms in the phytoplankton community. This is exactly the region where our GWR model revealed the lowest scaling factor values.

In high-biomass conditions, especially with large cells like diatoms, pigments are less efficiently absorbing light due to self-shading and intracellular packaging. This so-called pigment packaging effect leads to lower *Chla*-specific absorption coefficients (Stæhr et al., 2004), which in turn reduces the scaling factors.

#### 4.4. Limitations and future work

Time series from selected monitoring stations support the validity of the GWR-based approach, showing strong agreement in both magnitude and seasonal trends of *Chla* concentrations. Nonetheless, discrepancies remain, particularly during early spring and late autumn phytoplankton blooms, which are consistently detected in *in situ* measurements but underestimated or missed in the S3OL2-based *Chla* estimates—most notably at stations 2 and 4. This has been reported before (Stæhr et al., 2023), and might be a direct consequence of not taking into account short-term and/or seasonal patterns of pigment absorption properties. Encompassing the seasonal component of dynamics into the method is desirable, but it is not sure that the current frequency and coverage of *in situ Chla* data in space and time is sufficient to support spatio-temporal calibration of scaling factors.

To get a rough impression of seasonality impacts, we applied a  $\pm 45$  days moving window geometric mean regression for the entire matchup dataset sorted by day-of-the-year (suppl. Fig. S21). We can see a general seasonality with higher scaling factors in spring and autumn and lower ones during summertime. Applying this overall seasonal pattern of scaling factors improves statistical metrics compared to the global regression ( $R = 0.61$ ,  $RMSE = 0.28$ ), but to a lower extent than the spatial component, which we focused on in this study.

The new method in its recent form has only been tested for Danish Seas, is limited to areas with dense *in situ Chla* data, and only addresses spatial gradients. Therefore, we anticipate future studies extending the spatial scope to other regions, addressing temporal/seasonal dynamics and trends, as well as trying to describe the identified relationships from an ecological mechanistic perspective. If the widely variable *Chla*-specific absorption properties of phytoplankton (see Section 4.3) could be described mechanistically by geographic and/or physico-chemical data, appropriate spatial models for the scaling-factors  $Chl_{exp}$  and  $Chl_{fact}$  could be derived even for *in situ* data-poor areas.

## 5. Conclusions and perspectives

This study presents a novel approach to improving the accuracy of *Chla* estimations in complex coastal waters using S3OL2 C2RCC data. By employing advanced GWR modelling, scaling factors were spatially optimized, aligning the satellite-derived IOP  $a_{pig}^{443}$  with *in situ Chla* data from Denmark's national monitoring program (NOVANA). The GWR approach significantly enhances the correlation between satellite-based *Chla* estimates and *in situ* measurements, thus outperforming widely used C2RCC and OC4ME algorithms, for which issues with biased results have been reported. Our findings demonstrate that regionally tuned scaling factors can provide more reliable *Chla* estimates, supporting better marine ecosystem management and compliance with EU directives on eutrophication assessment. Our methodology offers a transparent, reproducible, and operationally feasible framework. It is transferable to other regions, satellite sensors, and parameters and may pave the way for more accurate and effective satellite-based marine monitoring strategies.

### CRedit authorship contribution statement

**Andreas Holbach:** Writing – review & editing, Writing – original draft, Visualization, Validation, Supervision, Software, Resources, Project administration, Methodology, Investigation, Funding acquisition, Formal analysis, Data curation, Conceptualization. **Sanjina Upadhyay Stæhr:** Writing – review & editing, Writing – original draft, Methodology, Investigation, Data curation. **Peter Anton Upadhyay Stæhr:** Writing – review & editing, Writing – original draft, Methodology, Conceptualization. **Stiig Markager:** Writing – review & editing, Resources, Methodology, Funding acquisition, Conceptualization.

### Declaration of Generative AI and AI-assisted technologies in the writing process

During the preparation of this work the authors used Microsoft Co-Pilot to improve readability and make parts of the text fit with the journal's formatting requirements. After using this tool, the authors thoroughly reviewed and edited the content as needed and take full responsibility for the content of the publication.

### Declaration of competing interest

The authors declare that they have no known competing financial interests or personal relationships that could have appeared to influence the work reported in this paper.

### Acknowledgements

This work was partly funded by (1) the 'Danish Agency for Green Transition and Aquatic Environment', (former The Danish Environmental Protection Agency) in the frame of the IMM (Integrated Marine environmental Monitoring) project, and the (2) OBAMA-NEXT (observing and mapping marine ecosystems — next generation tools) project, which is funded by the European Union under the Horizon Europe programme (grant agreement no. 101081642).

### Appendix A. Supplementary data

Supplementary data to this article can be found online at <https://doi.org/10.1016/j.scitotenv.2025.180868>.

### Data availability

All the data used in this study are already publicly available and data sources specified.

## References

- Bracher, A., Banks, A.C., Xi, H., Dessailly, D., Gossn, J., Lebreton, C., et al., 2025a. Assessment of OLCI absorption coefficients for non-water components across all optical water classes. *Front. Remote Sens.* 6.
- Bracher, A., Sopha, M.A., Banks, A.C., Xi, H., Chaikalis, S., Röttgers, R., 2025b. Absorption Coefficients by Phytoplankton at the First Eight Ocean Land Colour Instrument (OLCI) Bands from a Global In-Situ Collection of Open Ocean, Coastal and Inland Surface Waters Matched to OLCI. PANGAEA.
- Brockmann, C., Dury, S., Hesselmanns, G., Hakvoort, H., Duin, R.N.M., Slater, M.T., et al., 2004. Operational Coastal Water Quality Monitoring: Are Space Borne Products an Alternative to in-Situ Measurements - where Are we Now?.
- Brockmann, C., Doerffer, R., Peters, M., Stelzer, K., Embacher, S., Ruescas, A., 2016. Evolution of the C2RCC neural network for sentinel 2 and 3 for the retrieval of ocean colour products in normal and extreme optically complex waters. *Living Planet Symposium* 740, 54.
- Cazzaniga, I., Bresciani, M., Colombo, R., Della Bella, V., Padula, R., Giardino, C., 2019. A comparison of Sentinel-3-OLCI and Sentinel-2-MSI-derived chlorophyll-a maps for two large Italian lakes. *Remote Sens. Lett.* 10, 978–987.
- Charlton, M., Fotheringham, S., 2009. In: National Centre for Geocomputation NUoIM (Ed.), *Geographically Weighted Regression*.
- Chu, H.-J., Kong, S.-J., Chang, C.-H., 2018. Spatio-temporal water quality mapping from satellite images using geographically and temporally weighted regression. *Int. J. Appl. Earth Obs. Geoinf.* 65, 1–11.
- Ciotti, A.M., Lewis, M.R., Cullen, J.J., 2002. Assessment of the relationships between dominant cell size in natural phytoplankton communities and the spectral shape of the absorption coefficient. *Limnol. Oceanogr.* 47, 404–417.
- Danish Agency for Climate Data, 2025. Topografisk Landpolygon.
- Danish Geodata Agency, 2024. Denmark's Depth Model, 50 m Resolution.
- Doerffer, R., 2010. OLCI Level 2 - Algorithm Theoretical Basis Document. Ocean Colour Turbid Water.
- Doerffer, R., Embacher, S., 2016. c2rcc.olci (v.2.1).
- EMODnet Bathymetry Consortium, 2022. EMODnet Digital Bathymetry (DTM 2022), Tiles D4, D5, D6.
- ESA, 2020. ESA. Sentinel Application Platform (SNAP) 8.0.
- EU, 2000. Directive 2000/60/EC of the European Parliament and of the Council of 23 October 2000 Establishing a Framework for Community Action in the Field of Water Policy.
- EU, 2008. Directive 2008/56/EC of the European Parliament and of the Council of 17 June 2008 Establishing a Framework for Community Action in the Field of Marine Environmental Policy (Marine Strategy Framework Directive) (Text with EEA relevance), pp. 19–40.
- EUMETSAT, 2024. Sentinel-3 ocean colour level 2 data guide.
- Gholizadeh, H., Robeson, S.M., 2016. Revisiting empirical ocean-colour algorithms for remote estimation of chlorophyll-a content on a global scale. *Int. J. Remote Sens.* 37, 2682–2705.
- Hammond, M.L., Henson, S.A., Lamquin, N., Clerc, S., Donlon, C., 2020. Assessing the effect of tandem phase Sentinel-3 OLCI sensor uncertainty on the estimation of potential ocean chlorophyll-a trends. *Remote Sens.* 12.
- Hansen, J.W., Høgslund, S., 2021. Marine områder 2020. NOVANA. Aarhus Universitet, DCE – Nationalt Center for Miljø og Energi.
- Harvey, E.T., Kratzer, S., Philipson, P., 2015. Satellite-based water quality monitoring for improved spatial and temporal retrieval of chlorophyll-a in coastal waters. *Remote Sens. Environ.* 158, 417–430.
- Henriksen, P., 2009. Long-term changes in phytoplankton in the Kattegat, the Belt Sea, the sound and the western Baltic Sea. *J. Sea Res.* 61, 114–123.
- Holbach, A., Staehr, S.U., Staehr, P.A.U., Markager, S., 2025. Estimating underwater light attenuation from space - a spectral approach for case 2 marine waters. *Sci. Total Environ.* 986, 179775.
- IPCC, 2019. The ocean and cryosphere in a changing climate. In: *Intergovernmental Panel on Climate Change*, Cambridge, UK and New York, NY, p. 755.
- Kowalczyk, P., Stedmon, C.A., Markager, S., 2006. Modeling absorption by CDOM in the Baltic Sea from season, salinity and chlorophyll. *Mar. Chem.* 101, 1–11.
- Kratzer, S., Plowey, M., 2021. Integrating mooring and ship-based data for improved validation of OLCI chlorophyll-a products in the Baltic Sea. *Int. J. Appl. Earth Obs. Geoinf.* 94.
- Kutser, T., Soomets, T., Toming, K., Uiboupin, R., Arikas, A., Vahter, K., et al., 2018. Assessing the Baltic Sea water quality with Sentinel-3 OLCI imagery. *IEEE/OES Baltic International Symposium (BALTIC)* 2018, 1–6.
- Kyryliuk, D., Kratzer, S., 2019. Evaluation of sentinel-3A OLCI products derived using the Case-2 regional CoastColour processor over the Baltic Sea. *Sensors (Basel)* 19.
- Ligi, M., Kutser, T., Kallio, K., Attila, J., Koponen, S., Paavel, B., et al., 2017. Testing the performance of empirical remote sensing algorithms in the Baltic Sea waters with modelled and in situ reflectance data. *Oceanologia* 59, 57–68.
- Liu, B., D'Sa, E.J., Maiti, K., Rivera-Monroy, V.H., Xue, Z., 2021. Biogeographical trends in phytoplankton community size structure using adaptive sentinel 3-OLCI chlorophyll a and spectral empirical orthogonal functions in the estuarine-shelf waters of the northern Gulf of Mexico. *Remote Sens. Environ.* 252, 112154.
- Maar, M., Markager, S., Madsen, K.S., Windolf, J., Lyngsgaard, M.M., Andersen, H.E., et al., 2016. The importance of local versus external nutrient loads for Chl a and primary production in the Western Baltic Sea. *Ecol. Model.* 320, 258–272.
- Markager, S., Fossing, H., 2013. Klorofyl a koncentration - Teknisk anvisning. Teknisk Anvisning. Aarhus University DCE - Danish Centre For Environment And Energy, p. 10.
- Martin, S., 2014. An Introduction to Ocean Remote Sensing. Cambridge University Press, Cambridge.
- Mélin, F., Vantrepotte, V., 2015. How optically diverse is the coastal ocean? *Remote Sens. Environ.* 160, 235–251.
- Nazeer, M., Bilal, M., 2018. Evaluation of ordinary least square (OLS) and geographically weighted regression (GWR) for water quality monitoring: a case study for the estimation of salinity. *J. Ocean Univ. China* 17, 305–310.
- O'Kane, S., McCarthy, T., Fealy, R., Kratzer, S., 2024. A validation of OLCI Sentinel-3 water products in the Baltic Sea and an evaluation of the effect of system vicarious calibration (SVC) on the Level-2 water products. *Remote Sens.* 16.
- Olli, K., Klais, R., Tamminen, T., Ptacnik, R., Andersen, T., 2011. Long term changes in the Baltic Sea phytoplankton community. *Boreal Environ. Res.* 16, 3–14.
- Pitarch, J., Volpe, G., Colella, S., Krasemann, H., Santoleri, R., 2016. Remote sensing of chlorophyll in the Baltic Sea at basin scale from 1997 to 2012 using merged multi-sensor data. *Ocean Sci.* 12, 379–389.
- Riemann, B., Carstensen, J., Dahl, K., Fossing, H., Hansen, J.W., Jakobsen, H.H., et al., 2015. Recovery of Danish coastal ecosystems after reductions in nutrient loading: a holistic ecosystem approach. *Estuar. Coasts* 39, 82–97.
- Smith, V.H., 2003. Eutrophication of freshwater and coastal marine ecosystems: a global problem. *Environ. Sci. Pollut. Res. Int.* 10, 126–139.
- Stæhr, P.A., Markager, S., 2004. Parameterization of the chlorophyll a-specific in vivo light absorption coefficient covering estuarine, coastal and oceanic waters. *Int. J. Remote Sens.* 25, 5117–5130.
- Stæhr, P.A., Markager, S., Sand-Jensen, K., 2004. Pigment specific in vivo light absorption of phytoplankton from estuarine, coastal and oceanic waters. *Mar. Ecol. Prog. Ser.* 275, 115–128.
- Staehr, S.U., Van der Zande, D., Staehr, P.A.U., Markager, S., 2022. Suitability of multisensory satellites for long-term chlorophyll assessment in coastal waters: a case study in optically-complex waters of the temperate region. *Ecol. Indic.* 134.
- Staehr, S.U., Holbach, A.M., Markager, S., Staehr, P.A.U., 2023. Exploratory study of the Sentinel-3 level 2 product for monitoring chlorophyll-a and assessing ecological status in Danish seas. *Sci. Total Environ.* 897, 165310.
- Strong, J.A., Elliott, M., 2017. The value of remote sensing techniques in supporting effective extrapolation across multiple marine spatial scales. *Mar. Pollut. Bull.* 116, 405–419.
- Toming, K., Kutser, T., Uiboupin, R., Arikas, A., Vahter, K., Paavel, B., 2017. Mapping water quality parameters with Sentinel-3 ocean and land colour instrument imagery in the Baltic Sea. *Remote Sens.* 9.
- Tran, M.D., Vantrepotte, V., Loisel, H., Oliveira, E.N., Tran, K.T., Jorge, D., et al., 2023. Band ratios combination for estimating chlorophyll-a from Sentinel-2 and Sentinel-3 in coastal waters. *Remote Sens.* 15.
- York, D., 1968. Least squares fitting of a straight line with correlated errors. *Earth Planet. Sci. Lett.* 5, 320–324.